ChemComm

Accepted Manuscript

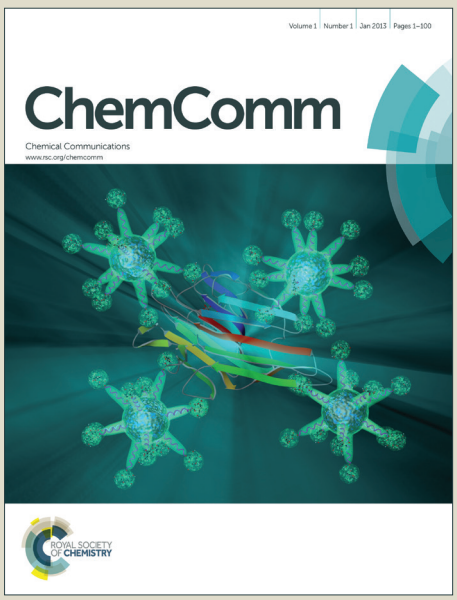

ROYAL SOCIETY OF CHEMISTRY

www.rsc.org/chemcomm

Chemical Communications RSCPublishing

COMMUNICATION

Ternary synthesis of colloidal Zn_3P_2 quantum dots

Cite this: DOI: 10.1039/x0xx00000x

Benjamin A. Glassy and Brandi M. Cossairt*

Received 00th January 2012,
Accepted 00th January 2012

DOI: 10.1039/x0xx00000x

www.rsc.org/

The synthesis and characterization of crystalline colloidal zinc phosphide quantum dots with observable excitonic transitions ranging between 424-535 nm (2.3-2.9 eV) are reported. A combination of $ZnEt_2$, $Zn(O_2CR)_2$, and $P(SiMe_3)_3$, is required for this synthesis. The ternary mixture initially forms a pentanuclear zinc cluster on mixing followed by conversion to $(Et_2Zn)P(ZnO_2CR)_2(SiMe_3)$ in a rate-determining step prior to quantum dot formation.

Rising global energy demands and diminishing fossil fuel reserves necessitate innovation in alternative energy sources. Solar radiation is promising given it is environmentally benign and abundant, but the high cost of solar cell fabrication and materials, particularly high quality crystalline silicon, prevents wide-spread deployment into the power grid.[1, 2] A recent cost-benefit analysis was performed on 23 semiconducting materials with electronic structures suitable for photovoltaic applications to determine possible alternatives to crystalline silicon. The study used the earth abundance of the semiconducting materials, raw material extraction costs, and theoretical efficiency of solar energy conversion based on band gap to determine their energy production potential. Of the 23 materials examined, nine were found to have the capacity to meet or exceed annual worldwide electricity consumption with a significant cost-reduction over crystalline silicon.[3] Among the most promising of these nine materials was zinc phosphide.

Zinc phosphide (Zn_3P_2) is ideally positioned as a next generation photovoltaic material as it has a direct band gap of 1.50 eV, which allows it to absorb a high percentage of the solar spectrum.[4] Zinc phosphide also has a high extinction coefficient,[5] and a long minority-carrier diffusion length (5-10 μm); properties that are desirable in efficient photovoltaic materials.[6] High-quality epitaxially grown Zn_3P_2 was first reported in 1992,[7] and heterojunction optoelectronic devices made with zinc phosphide have been fabricated, demonstrating the viability of industrial scale development of zinc phosphide semiconductor technologies.[8-11] However, for cost-effective large-scale synthesis, solution processable device fabrication, and control over the optical and electronic band gap, a colloidal quantum dot (QD) synthesis is desirable.[12, 13]

To date, there have been seven accounts of colloidal syntheses of Zn_3P_2.[14-20] The earliest study showed formation of zinc phosphide clusters with a distinct lowest energy excitonic transition (LEET) at 300 nm, indicative of relatively uniform crystalline particles, with an approximated 1 nm diameter. However, larger particles could not be obtained by this method.[14] Green and O'Brien describe a synthesis that gives a broad excitonic feature below 500 nm, but analysis showed a high degree of polydispersity and a mixture of crystalline and amorphous material.[16] Recent investigations have yielded zinc phosphide with no clear excitonic features in the absorption spectra and conflicting powder diffraction data, suggesting isolation of different crystal phases of zinc phosphide with a broad size distribution and lack of quantum confinement.[18, 19] These inconsistencies highlight the need for new, robust, and reproducible synthetic methods to obtain colloidal zinc phosphide quantum dots that are phase-pure, absorb in the visible region of the electromagnetic spectrum, and have low polydispersity.[21]

The reported synthetic approaches to colloidal zinc phosphide utilize a zinc precursor (zinc perchlorate,[14] zinc alkoxide,[15] zinc nanoparticles,[17] dialkylzinc,[16, 18-20] zinc stearate,[18] or zinc silylamide[18]), a phosphorus precursor (phosphine gas,[14, 18] tristrimethylsilylphosphine,[15, 18, 20] ditertbutylphosphine,[16] white phosphorus,[17] or trioctylphosphine[19, 20]), and excess ligands such as hexametaphosphate,[14] pyridine,[15, 16] trioctylphosphine,[16-20] or stearate.[18] This communication discusses a novel synthesis that relies on the *in situ* generation of a highly reactive pentanuclear zinc cluster from $ZnEt_2$ and $Zn(O_2CR)_2$ (R = $(CH_2)_{12}CH_3$ [MA] or $C(CH_2)_7CH{=}CH(CH_2)_7CH_3$ [OA]) followed by its *in situ* reaction with $P(SiMe_3)_3$ to generate $(Et_2Zn)P(ZnO_2CR)_2(SiMe_3)$ prior to conversion to zinc phosphide. The molecular precursor conversion is probed using ^1H and $^{31}P\{^1H\}$ NMR spectroscopy. Through control of the reaction temperature during nanocrystal growth, crystalline particles with clear excitonic transitions in the visible are obtained. Detailed characterization of the structure and composition of the resulting zinc-rich zinc phosphide nanocrystals by HRTEM, TEM, ICP-OES, TGA, NMR, and powder XRD are presented.

Our strategy to avoid the difficulties in forming this covalent material was to pre-form a cluster containing Zn−P bonds, with initial focus on silylphosphine and alkylzinc reagents inspired by an unusual Zn_6P_4 cluster observed by Arno Pfitzner and co-workers.[22] Our best results were obtained by injecting a mixture of $ZnEt_2$ and

$P(SiMe_3)_3$ into $Zn(O_2CR)_2$ at 100 °C followed by heating to the growth temperature (Scheme 1). UV-vis spectra of timed aliquots for a typical synthesis (Figure 1A) show the progression of the LEET as a function of temperature and time. Particles with a clear excitonic feature only formed when utilizing this heat-up method and all three precursors.[23]

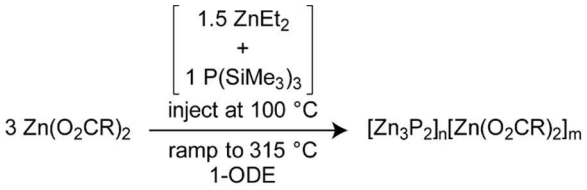

Scheme 1. Synthesis of zinc-rich zinc phosphide quantum dots from $ZnEt_2$, $Zn(O_2CR)_2$ where R = $(CH_2)_{12}CH_3$ or $C(CH_2)_7CH{=}CH(CH_2)_7CH_3$, and $P(SiMe_3)_3$.

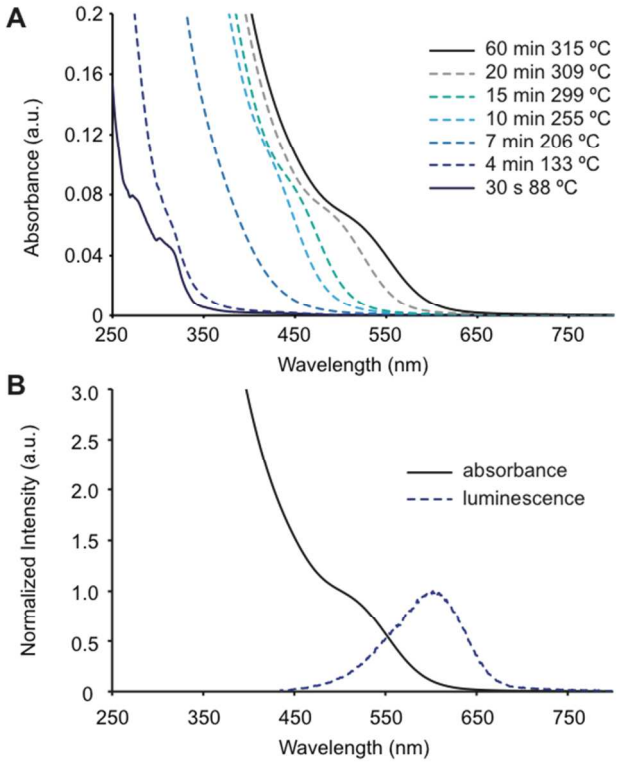

Figure 1. (A) UV-Vis spectra showing the temporal evolution of zinc phosphide quantum dots formed using Scheme 1. (B) Absorbance and room temperature photoluminescence of isolated zinc phosphide quantum dots.

The position of the final LEET is dependent on the final growth temperature achieved and ranged from 424 to 535 nm, with absorption onsets extending beyond 600 nm (Figure S2).[24] Photoluminescence (PL) was observed for all samples grown to temperatures ≥ 255 °C and was red shifted from the absorbance peak by at least 0.37 eV (Figures 1B and S3). The red shift in fluorescence and the lack of correlation of the emission profile from the absorption maxima suggests luminescence from mid-gap trap states.[18] The PL quantum yield of the synthesized Zn_3P_2 was 1%, typical of related metal phosphide systems.[18, 25, 26]

Experiments probing the effect of concentration on the synthesis indicated that a lower total concentration dramatically increased the energy of the LEET (Figure S4). This is in line with classical nucleation theory whereby a greater fraction of the available monomer reserves are consumed during the nucleation event leaving less available monomers for further growth in a low total concentration scenario.[27, 28]

NMR experiments were conducted to elucidate the mechanism of precursor conversion and to understand the synergistic role of using two different zinc precursors. A series of control experiments were first performed to determine the individual roles of each molecular precursor. When $P(SiMe_3)_3$ and $ZnEt_2$ were combined in C_6D_6 in a J-Young tube, the ^1H and $^{31}P\{^1H\}$ NMR spectra reveal no change over the course of 24 hours at room temperature. There is also no change at 80 °C over the course of one hour (Figure S5). These results suggest that $P(SiMe_3)_3$ does not directly react with $ZnEt_2$ under these conditions. In C_6D_6, $P(SiMe_3)_3$ and $Zn(O_2CR)_2$ react over the course of hours (half-life of 5 hours for R = CH_3) at room temperature and do not form any resolvable phosphorus containing intermediates (Figure S6). Zinc carboxylates and diethyl zinc, however, are known to react to form $[Zn_5(O_2CR)_6(Et)_4]$ clusters in non-coordinating solvent, and we have identified this species in our the ^1H NMR data (Figure S7).[29] When $P(SiMe_3)_3$ is combined with this pre-formed zinc cluster, it reacts on the order of minutes (half-life of < 5 minutes) to form a phosphorus-containing intermediate with a chemical shift of −276 ppm (Figure S8).

To probe the molecular transformation of all three precursors, $Zn(MA)_3$, $P(SiMe_3)_3$, and $ZnEt_2$ were mixed in a J-Young tube at room temperature in C_6D_6 and was monitored by $^{31}P\{^1H\}$ and ^1H NMR spectroscopy. The time resolved $^{31}P\{^1H\}$ NMR spectra show the disappearance of the $P(SiMe_3)_3$ singlet at −252 ppm along with the concomitant appearance of a new singlet at −276 ppm, which suggests that $P(SiMe_3)_3$ is converting to a new molecular species over the period of hours at 22 °C (Figure S9). The ^1H NMR spectra are difficult to analyze due to the overlapping peaks from the myristate ligands, however the complexity of the ^1H NMR spectra can be significantly reduced by replacing $Zn(MA)_2$ with $Zn(Ac)_2$ (Ac = O_2CCH_3).

When $Zn(Ac)_2$, $P(SiMe_3)_3$, and $ZnEt_2$ are combined in C_6D_6 in a J-Young NMR tube at room temperature, the reaction mixture is initially heterogeneous due to the insolubility of $Zn(Ac)_2$ in C_6D_6, but becomes homogenous over time. The time resolved $^{31}P\{^1H\}$ NMR spectra show the formation and disappearance of a singlet at −276 ppm, as observed when using $Zn(MA)_2$ (Figure 2A). This reaction also has a corresponding resolvable ^1H NMR spectrum which shows the formation and disappearance of the proposed phosphorus-containing intermediate in addition to the pentanuclear $[Zn_5(Ac)_6(Et)_4]$ cluster, and the silylacetate co-product (Figure 2B). Based upon the integration of a ^1H NMR spectrum taken two hours after all three precursors were mixed together (Figure S10), we propose that the long lived phosphorus containing intermediate is $(Me_3Si)P(ZnAc)_2$ with a $ZnEt_2$ group datively bound (Figure 2C). The assignment of P-bound $ZnEt_2$ is based on the observation of the downfield shift and broadening of free $ZnEt_2$ concomitant with the appearance of the phosphorus-containing intermediate in addition to its subsequent shift back and sharpening on loss of this intermediate. There is literature precedent for related tetrahedrally-coordinated phosphorus species displaying $^{31}P\{^1H\}$ NMR signals at −318.5[30] and −270.3[31] ppm. We were unable to isolate and purify the proposed $(Et_2Zn)P(ZnAc)_2(SiMe_3)$ species due to its limited lifetime and instability under reduced pressure. The observed intermediate with a $^{31}P\{^1H\}$ NMR peak at −276 ppm was also implicated as the species directly responsible for the formation of QDs in a typical heat-up synthesis. This intermediate was the only molecular species containing phosphorus observed by $^{31}P\{^1H\}$ NMR in an aliquot taken 30 seconds post injection from a typical synthesis (Figure S11) and no phosphorus containing molecular species were observed by $^{31}P\{^1H\}$ NMR in an aliquot taken after Zn_3P_2 QD formation. These observations indicate the loss of the intermediate observed at −276

ppm by $^{31}P\{^{1}H\}$ NMR directly correlates with the formation of QDs and is not a by-product of the reaction. To further support this hypothesis, a QD synthesis was performed in a J-Young tube to monitor the formation and disappearance of the observed molecular intermediate during QD formation. In this experiment $Zn(MA)_2$, $ZnEt_2$, and $P(SiMe_3)_3$ were mixed in 1-ODE in a J-Young tube and heated up in a sand bath and $^{31}P\{^{1}H\}$ NMR spectra were taken after the NMR tube had been heated to various temperatures. This series of $^{31}P\{^{1}H\}$ NMR spctra show the growth of the intermediate species at −276 ppm followed by its gradual disappearance, suggesting that this species is active in QD formation and is the only long-lived phosphorous containing molecular precursor observable prior to QD formation (Figure S12).

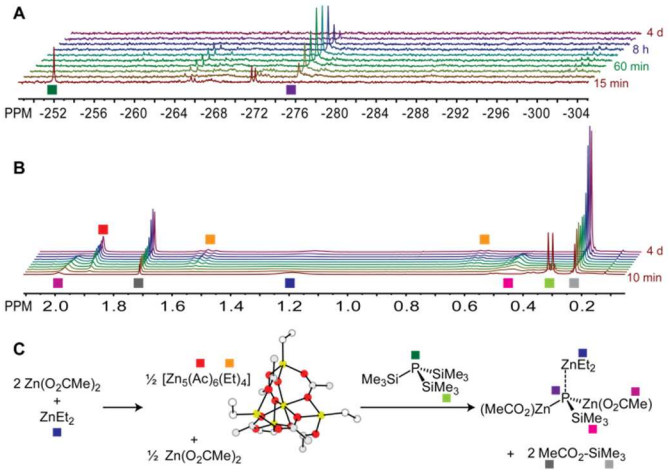

Figure 2. (A) $^{31}P\{^{1}H\}$ NMR spectra showing time evolution of the zinc phosphide precursor conversion reactions at 22 °C. (B) ^{1}H NMR spectra showing the corresponding time evolution of the zinc phosphide precursor conversion reactions at 22 °C. (C) Proposed scheme for the zinc phosphide precursor conversion reactions.

Further evidence in support of this hypothesis resulted from pre-mixing all three molecular precursors ($Zn(MA)_2$, $ZnEt_2$, and $P(SiMe_3)_3$) in 3 grams of 1-ODE at room temperature until complete conversion to the molecular species with a $^{31}P\{^{1}H\}$ NMR resonance at –276 ppm was observed (8 hours). This solution, containing the pre-formed precursor, was injected into 5 grams of 1-ODE at 100 °C and heated to 315 °C. The formation of Zn_3P_2 QDs was observed, similar to a typical synthesis in which this species was not purposely pre-formed (Figure S13). To corroborate our hypothesis that the pentanuclear zinc cluster (Figure 2C) forms first in a typical synthesis, a QD reaction was performed in which there was a 15 minute delay between injecting $ZnEt_2$ and $P(SiMe_3)_3$ into a $Zn(OA)_2$ solution in 1-ODE in a three neck flask prior to heating up to 315 °C (Figure S14). The size and spectroscopic characteristics of the particles formed in this experiment were within error of particles formed when $ZnEt_2$ and $P(SiMe_3)_3$ are introduced simultaneously.

The results of these experiments are consistent with the postulate that in the ternary synthesis, a pentanuclear zinc cluster is initially formed via reaction of $Zn(O_2CR)_2$ with $ZnEt_2$. The rate of reaction between $[Zn_5(O_2CR)_6(Et)_4]$ with $P(SiMe_3)_3$ is greatly enhanced relative to $ZnEt_2$ or $Zn(O_2CR)_2$ alone, and this reaction leads to formation of the long-lived $(Et_2Zn)P(ZnO_2CR)_2(SiMe_3)$ intermediate with a ^{31}P NMR signal at −276 ppm. This species is the key molecular precursor preceding nucleation and growth of the reported Zn_3P_2 QDs.

Transmission electron microscopy (TEM) images were collected to determine the average particle size of the Zn_3P_2 QDs. Quantum dots grown to 315 °C (LEET at 535 nm) had an average diameter of 2.9 ± 0.6 nm based upon measurements made on 300 individual particles using ImageJ[32] (Figure 3, histogram found in Figure S15),[33] while quantum dots grown to 255 °C (LEET at 424 nm) had an average diameter of 2.6 ± 0.5 nm (Figure S16). QDs grown to the two temperatures had average particle diameters within 0.3 nm, however the energy of the LEET from the UV-vis spectra differed by 0.6 eV, indicative of a high degree of quantum confinement. Calculation of the expected average particle size based on the energy of the LEET using the Brus equation with a range of reported reduced electron and hole masses predict this behavior, with a maximum difference in expected radius of 0.4 nm between the two samples.[34] Using the same range of electron and hole masses, the exciton Bohr radius of Zn_3P_2 was calculated to range between 3 and 7 nm.[35] This is consistent with our assignment of the Zn_3P_2 prepared here as quantum confined semiconductor nanocrystals. Particles formed without $ZnEt_2$ had an average diameter of 2.6 ± 0.5 nm (Figure S17), however these particles exhibit no excitonic features in the visible and the sample is likely largely amorphous (*vide infra*). High resolution TEM (HRTEM or phase-contrast TEM) was used to confirm the crystallinity and lattice spacing of QDs grown to 315 °C with all three precursors. FEI TrueImage software was used to reconstruct the exit wavefunction using a series of images taken at different focus points. Analysis of the particle shown in Figure 3 (left) showed lattice plane spacings of 2.6 and 1.6 Å which are consistent with the (301) and (051) planes of the tetragonal α-Zn_3P_2 phase, respectively.[36]

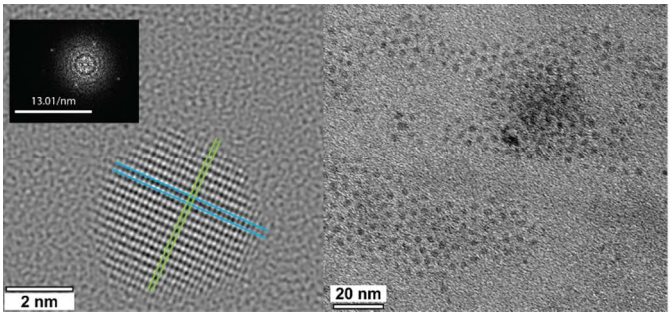

Figure 3. (Left) High resolution TEM image of a single zinc phosphide quantum dot with the FFT as an inset and (Right) low resolution TEM image of zinc phosphide quantum dots.

Air-free X-ray diffraction (XRD) was performed by sealing a solid sample of synthesized particles under a Kapton® film. The collected diffraction pattern (Figure S18) agrees favourably with the pattern for Zn_3P_2 (tetragonal α-Zn_3P_2; COD 1010287). Upon air oxidization, there is a change in diffraction pattern indicating these particles are air sensitive (Figure S19). An air-free pattern of particles synthesized without $ZnEt_2$ shows a very intense peak at 19° 2θ which could be indicative of poor crystallinity (Figure S20). Sherrer analysis was performed on the particles grown using all three precursors using both the peaks at 32° and 45° 2θ[37] and yielded an average particle diameter of 1.1 and 2.8 nm, the second of which is consistent with the TEM data (Figure S21) for a 0.4 mmol $P(SiMe_3)_3$ reaction.[38, 39] The peak at 32° 2θ was analyzed assuming one reflection was the sole cause of the intensity, which may not be the case. Also, given the small particle size, the surface will have a larger impact on lattice strain which would broaden the peak width.

Due to the similarity in the solubility of the zinc phosphide QDs and zinc myristate, particles synthesized with this zinc reagent could not be separated from excess zinc myristate. Zinc phosphide QDs were therefore prepared using more soluble zinc oleate for complete excess ligand removal. ^{1}H NMR data confirmed clean isolation of zinc-rich particles capped only by oleate ligands (Figure S22). Particles grown to 255 °C had a zinc to phosphorus ratio of 7.6:2 and

particles grown to 315 °C had a zinc to phosphorus ratio of 5:2 as determined by inductively coupled plasma atomic emission spectroscopy (ICP-OES). Thermogravimetric analysis (TGA) was performed under nitrogen on particles grown to 315 °C, showing a single weight loss transition centered near 400 °C. Following TGA, 46% inorganic mass remained, consistent with a $Zn(O_2CR)_2$-capped zinc phosphide formulation with less than a mono-layer of zinc oxide included at the surface (Figure S23).[33]

In order to assess the potential of these particles for photovoltaic applications, their photoresponse was measured. A film of particles was electrodeposited onto a conductive mesoporous *nano*ITO substrate[40] using electrophoretic deposition at 45 V from a toluene/acetonitrile solution of QDs under argon, followed by a one hour anneal under vacuum at 350 °C (Figure S24). Controlled potential electrolysis was performed under chopped white light (Figure S25) and showed a 100 nA current increase with light irradiation indicating the possibility of using these particles as visible light absorbers.[33] A detailed study of the electrical properties of surface-treated zinc phosphide nanocrystals is underway.

In Conclusion, this work describes a novel three precursor synthesis of colloidal crystalline Zn_3P_2 quantum dots that have clear excitonic absorbance features ranging from 424 to 535 nm, depending on the final growth temperature. NMR experiments revealed a critical molecular transformation that only occurs when $ZnEt_2$, $Zn(O_2CR)_2$, and $P(SiMe_3)_3$ are all present. The observed $(Et_2Zn)P(ZnO_2CR)_2(SiMe_3)$ intermediate was conclusively shown to be a direct precursor to the crystalline zinc phosphide quantum dots obtained in this study. TEM, ICP-OES, TGA, NMR, and XRD experiments showed that the resulting particles were crystalline and confirmed their identity as zinc-rich zinc phosphide QDs that ranged from 2.6 to 2.9 nm in diameter. In contrast to the synthesis of Zn_3P_2 QDs recently reported by Buriak and co-workers which yields 15 ± 2 nm particles from a combination of $ZnMe_2$ and $P(SiMe_3)_3$ with no strongly passivating ligands present, our synthesis yields relatively monodisperse colloidal solutions of small size nanocrystals as a result of carboxylate ligand passivation.[20] The stark contrast between the nanocrystal sizes reported here and by Buriak highlights the critical role of precursor reactivity and ligand binding strength on final particle size, and suggests a strategy for achieving nanocrystals of intermediate size.[41] Initial photoresponse measurements demonstrated the possibility of using these particles as visible light absorbers. Future experiments will focus on synthesizing and characterizing larger particles that retain an excitonic feature as well as fabricating solid state devices to probe the effect of QD composition and surface chemistry on device characteristics.

We gratefully acknowledge the University of Washington Department of Chemistry for support of this work. Part of this work was conducted at the University of Washington NanoTech User Facility, a member of the NSF National Nanotechnology Infrastructure Network (NNIN). We thank Scott Braswell for his help with TEM and HRTEM data collection. This research was supported by start-up funds from the University of Washington and the University of Washington Innovation Award.

Notes and references

University of Washington, Department of Chemistry, Box 351700, Bagley Hall, Seattle, WA 98195-1700.

*Corresponding author: cossairt@chem.washington.edu

Electronic Supplementary Information (ESI) available: The additional figures and information mentioned within this communication as well as details for all the experiments discussed can be found in the supplementary information document accompanying this communication. See DOI: 10.1039/c000000x/

1. R. R. Lunt, T. P. Osedach, P. R. Brown, J. A. Rowehl and V. Bulović, *Adv. Mater.*, 2011, **23**, 5712-5727.
2. A. E. Curtright, M. G. Morgan and D. W. Keith, *Environ. Sci. Technol.*, 2008, **42**, 9031-9038.
3. C. Wadia, A. P. Alivisatos and D. M. Kammen, *Environ. Sci. Technol.*, 2009, **43**, 2072-2077.
4. E. A. Fagen, *J. Appl. Phys.*, 1979, **50**, 6505-6515.
5. J. P. Bosco, S. B. Demers, G. M. Kimball, N. S. Lewis and H. A. Atwater, *J. Appl. Phys.*, 2012, **112**, 093703.
6. N. C. Wyeth and A. Catalano, *J. Appl. Phys.*, 1979, **50**, 1403-1407.
7. T. Suda and K. Kakishita, *J. Appl. Phys.*, 1992, **71**, 3039-3041.
8. M. Bhushan and A. Catalano, *Appl. Phys. Lett.*, 1981, **38**, 39-41.
9. P. S. Nayar and A. Catalano, *Appl. Phys. Lett.*, 1981, **39**, 105-107.
10. G. M. Kimball, N. S. Lewis and H. A. Atwater, Photovoltaic Specialists Conference (PVSC), 2010 35th IEEE, 2010.
11. R. Yang, Y.-L. Chueh, J. R. Morber, R. Snyder, L.-J. Chou and Z. L. Wang, *Nano Lett.*, 2006, **7**, 269-275.
12. C. B. Murray, D. J. Norris and M. G. Bawendi, *J. Am. Chem. Soc.*, 1993, **115**, 8706-8715.
13. L. Li, M. Protière and P. Reiss, *Chem. Mater.*, 2008, **20**, 2621-2623.
14. H. Weller, A. Fojtik and A. Henglein, *Chem. Phys. Lett.*, 1985, **117**, 485-488.
15. W. E. Buhro, *Polyhedron*, 1994, **13**, 1131-1148.
16. M. Green and P. O'Brien, *Chem. Mater.*, 2001, **13**, 4500-4505.
17. S. Carenco, M. Demange, J. Shi, C. Boissiere, C. Sanchez, P. Le Floch and N. Mezailles, *Chem. Commun.*, 2010, **46**, 5578-5580.
18. S. Miao, T. Yang, S. G. Hickey, V. Lesnyak, B. Rellinghaus, J. Xu and A. Eychmüller, *Small*, 2013, **9**, 3415-3422.
19. E. J. Luber, M. H. Mobarok and J. M. Buriak, *ACS Nano*, 2013, **7**, 8136-8146.
20. M. H. Mobarok, E. J. Luber, G. M. Bernard, L. Peng, R. E. Wasylishen and J. M. Buriak, *Chem. Mater.*, 2014, **26**, 1925-1935.
21. J. R. Heath and J. J. Shiang, *Chem. Soc. Rev.*, 1998, **27**, 65-71.
22. M. Westerhausen, G. Sapelza, M. Zabel and A. Pfitzner, *Z. Naturforsch. B*, 2004, **59**, 1548-1550.
23. See figure S1 for absorbance of particles made without diethyl zinc.
24. LEET is determined by fitting the spectra and taking the second-derivative to locate the local minima.
25. D. Battaglia and X. Peng, *Nano Lett.*, 2002, **2**, 1027-1030.
26. R. Wang, C. I. Ratcliffe, X. Wu, O. Voznyy, Y. Tao and K. Yu, *J. Phys. Chem. C*, 2009, **113**, 17979-17982.
27. V. K. LaMer and R. H. Dinegar, *J. Am. Chem. Soc.*, 1950, **72**, 4847-4854.
28. S. G. Kwon and T. Hyeon, *Small*, 2011, **7**, 2685-2702.
29. K. L. Orchard, A. J. P. White, M. S. P. Shaffer and C. K. Williams, *Organometallics*, 2009, **28**, 5828-5832.
30. O. Fuhr and D. Fenske, *Z. Anorg. Allg. Chem.*, 2004, **630**, 244-246.
31. G. Sapelza, P. Mayer and M. Westerhausen, *Z. Anorg. Allg. Chem.*, 2005, **631**, 3087-3091.
32. C. A. Schneider, W. S. Rasband and K. W. Eliceiri, *Nat. Methods*, 2012, **9**, 671-675.
33. See the ESI for experimental detials.
34. P. J. Reid, B. Fujimoto and D. R. Gamelin, *J. Chem. Educ.*, 2013, **91**, 280-282.
35. M. Kuno, in *Introductory Nanoscience: Physical and Chemical Concepts*, Garland Science: Taylor & Francis Group, New York, 2012, ch. **3**, pp. 29-60.
36. This larger than average particle gave the most detail during imaging.
37. The discrepancy in expected versus observed peak intensity for the 45 2θ reflection may be the result of a defective lattice and may be an indication of the zinc-rich nature of this sample.
38. P. Scherrer, *Nachr. Ges. Wiss. Göttingen.*, 1918, **1990**, 98-100.
39. M. G. Bawendi, A. R. Kortan, M. L. Steigerwald and L. E. Brus, *J. Chem. Phys.*, 1989, **91**, 7282-7290.
40. P. G. Hoertz, Z. Chen, C. A. Kent and T. J. Meyer, *Inorg. Chem.*, 2010, **49**, 8179-8181.
41. M. H. Mobarok and J. M. Buriak, *Chem. Mater.*, 2014, **26**, 4653-4661.

